

# TRIGGERING AND CONFINEMENT EFFECT OF 1D TO 3D CHAOTIC SOLITONS BY THE INTERPLAY OF PERIODIC SPATIO-TEMPORAL FIELDS

SORGE OPORTO-ALMARAZ, GERARDO F. MEYER-FORGUES  
CAMILO J. CASTRO, DETERLINO URZAGASTI

Facultad de Ciencias Puras y Naturales, Universidad Mayor de San Andrés  
Campus Universitario, Calle 27 Cota-Cota, P.O. Box 8635, La Paz, Bolivia

*(Received May 3, 2020; accepted October 21, 2020)*

We report on the triggering of localized and confined chaos described by a general cubic order damped nonlinear Schrödinger amplitude equation containing a conjugate amplitude term, representing the time-periodic parametric driving, and a spatially periodic term representing the external potential that cuts and confines the chaotic patterns promoted by the former, leading to trapped chaotic space-localized structures. Numerical simulations in  $1 + 1$ ,  $1 + 2$ , and  $1 + 3$  dimensions, Lagrangian and Hamiltonian theories for continuous fields, moments method, largest Lyapunov exponents, spectral distributions, and bifurcations diagrams are used to characterize and analyze these chaotic solitons.

DOI:10.5506/APhysPolB.51.2159

## 1. Introduction

All of physical phenomena are nonlinear in nature. Mechanics [1], fluid dynamics, plasma physics, gas dynamics, Bose–Einstein condensates [2, 3], magnetism [4, 5], cosmology [6], nonlinear optics [7–13], superconductivity [14], and water wave propagation [15, 16] are some of the many branches of science in which plenty of research is developed regarding nonlinear equations. This is the motivation for investigation in these fields, despite their analytical and mathematical complexity. The mathematical nonlinear analysis of complex systems is distinguished for the invalidity of the superposition principle, the nonexistence of a single solution, and the inaccuracy of the numerical approximations. This leads to the development of several techniques in order to characterize the solutions of these systems [17–22].

One of the most studied and important equations that describes nonlinear systems is the nonlinear Schrödinger equation (NLSE). It took great importance in 1950 when Ginzburg and Landau were studying the macroscopic theory of superconductivity [23, 24]. It was later seen that the NLSE could be applied to a wide variety of fields, including nonlinear optics, water waves, optical communications, photonics, plasmas, Bose–Einstein condensates, micromagnetism, semiconductor electronics, *etc.* [25–27]. The NLSE can be modified by the inclusion of several terms in order to account for different physical phenomena regarding a particular physical system under consideration [17, 28]. These terms can represent phenomena that are associated with dispersion, dissipation, energy injection, *etc.* It is important to note that, despite its name, the NLSE does not necessarily have a quantum interpretation, because only its mathematical structure is similar to the Schrödinger equation of quantum mechanics [29–32].

Solitons are typical NLSE solutions with the form of localized structures in space or time, which are stationary (although not necessarily motionless) in the case of integrable NLSEs [33], periodic, quasiperiodic with complex oscillations in the case of breathers [5], or chaotic, as in the case of dissipative solitons subject to significant external driving [34, 35]. To solve spatial systems, perhaps the simplest approach is to consider a stationary soliton with the shape of a hyperbolic-secant function [36–38]. It is well-known that this kind of initial conditions can lead to quasiperiodic or chaotic behavior [39], or even to spatio-temporal chaos [40].

Periodic potentials are widely studied in the context of nonlinear amplitude equations because of its importance as a model in several physical phenomena to describe a diverse complex behavior. The most important and numerically abundant effect of such potentials is nontrivial motion. These include seesaw oscillations [41] centering at or in-between potential valleys, and confinement in a single potential valley [27, 42–44]. Other noteworthy examples are splitting [45–47] and the emission of radiation by a nonstationary soliton [2, 27, 48, 49].

Alternate nonlinear amplitude equations include not only periodic potentials but also damping and parametric driving such as the parametrically-driven damped nonlinear Schrödinger equation [50, 51]; in fact, the interplay between dispersion and nonlinearity is characteristic of solitons. This type of systems allows the existence of structures such as standard and dissipative breather solitons, which are nonchaotic quasiperiodic localized patterns [5].

Soliton-bearing systems have been analytically studied using collective coordinate theories often called *method of moments*, which are equivalent to the variational Lagrangian method [52]. The results of both methods allow qualitative descriptions, where the agreement of such models and numerical simulations is often deemed appropriate when sufficiently small perturbations are considered [53].

These approaches allow the construction of nonintegrable many-particle soliton dynamics with an effective Hamiltonian which ultimately leads to chaos [54]. Employing particle models instead of the NLSE also allows the existence of chaotic dynamics for the three-soliton system [37]. Similar non-integrable problems, such as coupled nonlinear Schrödinger equations, exhibit solitons which are surrounded by chaotic regions [55].

Experimental evidence of chaotic solitons has been reported [56, 57] and modeled in different contexts of pulsatile, periodic and/or chaotic soliton dynamics (either in its structure [58] or its propagation [38]), and in phenomena such as breaking of spatial and temporal symmetry [59]. This dynamic wealth is associated with the nonintegrability of the system due to an increase in the degree of nonlinearity of the equations [58, 60] which include terms that take into account several factors, namely: the nature and geometry of the medium [36, 60, 61] as well as the potential associated with it [36, 37, 59, 62], the soliton–soliton interaction potentials [37, 63], the parametric forcing [5, 64], and gain–loss effects [58, 60]. The increase of the dimension and the coupling of solitons also influences the complexity of the system [38, 61].

The aim of this manuscript is to study the confined and localized chaos in dissipative systems with cubic nonlinearities originated by the joint action of external periodic spatial and temporal fields which, as far as we know, has not been yet reported in the literature. For this task, we use the model described by a general cubic order forced and parametrically-driven and damped nonlinear Schrödinger amplitude equation (cubic-FPDDNLSE) in 1+1 dimensions containing a conjugate amplitude term,  $\eta A^*$ , and a spatially periodic term,  $AN_0 \sin^2(Kx)$ , where  $A = A(x, t)$  is the complex amplitude function of the space-time coordinates,  $\eta$  is a constant that represents the intensity of a periodic temporal driving field, and where  $N_0$  and  $K$  are the amplitude and frequency of the periodic spatial field. Along with numerical simulations, Lagrangian and Hamiltonian formulations for continuous fields as well as the method of moments are used in order to characterize the localized solutions of the cubic-FPDDNLSE, and to analyze the impact of the external driving fields on the dynamical properties of these chaotic solitons.

Previous work has reported the existence of localized and chaotic domains triggered and confined by the action of periodic external forcing fields described by the cubic–quintic Ginzburg–Landau equation and for the specific case of optical fibers [44]. The case we study here is essentially different, since apart from being of cubic order, the existence of the dissipative soliton is achieved by the action of the periodic temporal field, which, when increasing in magnitude, originates the formation of an extended chaotic pattern that expands indefinitely [5], unless it is trapped and confined by a periodic spatial field in the form of a chaotic soliton (not domain). This is the motivation for the present work.

In addition, the confinement effects in  $1 + 2$  and  $1 + 3$  dimensions are also briefly explored, considering for this purpose the actions of a 2D and a 3D hexagonal spatial field, respectively.

This manuscript is organized as follows: in Section 2, the theoretical model is developed; in Section 3, the results are presented and discussed; and in Section 4, the concluding remarks are summarized.

## 2. Theoretical framework

### 2.1. Model equation

We consider a general model of amplitude equations consisting of the collection of some variants of the nonlinear Schrödinger equation, which apply to several problems in different physical contexts. This general form is the cubic-FPDDNLSE

$$i\partial_t A - \sigma \partial_x^2 A + \gamma |A|^2 A = (\nu - i\mu)A + i\eta A^* - AN_0 \sin^2(Kx), \quad (1)$$

where  $A = A(x, t)$  is the complex amplitude, which is a function of spatial and temporal coordinates  $(x, t)$ , and where  $(*)$  denotes the complex conjugation. For  $\sigma = 1$ , and  $\nu = \mu = \eta = N_0 = 0$ , we have the standard (or conservative) nonlinear Schrödinger equation (NLSE) [26]. For  $\sigma = 1$ ,  $\gamma = -1$ , and  $N_0 = 0$ , we have the parametrically-driven and damped nonlinear Schrödinger equation (PDDNLSE), where  $\mu$  is the damping parameter,  $\eta$  is the driving parameter, and  $\nu$  is the detuning parameter (or frequency adjustment parameter). This is the case, *e.g.*, within the context of studying precession states in parametrically-driven magnetic systems [5, 65] or when studying a vertically driven damped chain of pendula in the continuum limit [66]. For  $\eta = 0$ ,  $\gamma > 0$ , and  $N_0 = 0$ , we have the case of an NLSE that describes the behavior of the amplitude of the electric field that propagates in optical fibers, being  $\gamma$  the Kerr parameter, and, depending on the sign of  $\sigma$ , we have the normal dispersion regime ( $\sigma = 1$ ), or the anomalous dispersion regime ( $\sigma = -1$ ). The sine-squared term represents an external periodic forcing of amplitude  $N_0$  and frequency  $K$ . The form chosen for the latter is the simplest one that can be treated both analytically and numerically.

As an example, a physical model that can be described by Eq. (1) is a parametrically-driven and forced damped pendula chain, where the angle  $\phi(x', t')$  between a pendulum and the vertical axis in the continuum limit is modeled by the equation

$$0 = \phi_{t't'} - \phi_{x'x'} + \mu' \phi_{t'} + (\omega_0^2 + \delta^2 [h \sin^2(kx') + \gamma' \sin(\Omega t')]) \sin \phi, \quad (2)$$

where  $x'$  is the horizontal coordinate,  $t'$  the time,  $\mu'$  the dissipation coefficient,  $\omega_0^2$  the squared natural frequency, which is perturbed in the pendulum

length by a periodic in time vertical driving [66] of amplitude  $\delta^2\gamma'$  and by a vertical periodic in space forcing [67] of amplitude  $\delta^2h$ , being  $\delta^2$  the smallness order parameter. Working up to the cubic order, *i.e.* with  $\sin \phi \simeq \phi - \phi^3/6$  and around the parametric resonance:  $\Omega = -2\omega_0 + \nu'$ , being  $\nu'$  the detuning frequency, and replacing the Ansatz  $\phi = \delta A \exp(-i(\omega_0 + \nu'/2)t') + \text{c.c.}$  in Eq. (2), where  $A$  is the complex modulation amplitude of slow time variation (such that  $\partial_{t't'}A$  and  $(\partial_{t'}A)^2$  are neglected), we obtain, up to the  $\delta^2$  order and for the quasireversible case ( $\mu' \ll \omega_0$ ), our working equation, Eq. (1), with  $t = \delta^2 t'/2$ ,  $\sigma = 1$ ,  $x = \delta x' \sqrt{\omega_0}$ ,  $\nu = -\nu'/\delta^2$ ,  $\mu = \mu'/\delta^2$ ,  $\gamma = -\omega_0/2$ ,  $\eta = -\gamma'/2\omega_0$ ,  $N_0 = h/\omega_0$ , and  $K = k/\sqrt{\omega_0}\delta$ .

### 2.2. Lagrangian and Hamiltonian formalisms for the complex amplitude

Lagrangian and Hamiltonian formulations for continuous fields are widely used to study the NLSE and their variants whenever they could be derived from a variational principle [39, 52]. In this case, the Hamilton principle states that the dynamics of a physical system is determined by a functional  $\mathcal{L}$  called the Lagrangian density, which contains all the information about the system dynamics, regarding all the forces that act on it. The principle expresses that given the complex continuous field,  $A = A(x, t)$  (which in this case is our amplitude function), the action integral

$$S = \int \int \mathcal{L}(A, A^*, \partial_x A, \partial_x A^*, \partial_t A, \partial_t A^*; x, t) dx dt \tag{3}$$

is such that from its null variation,  $\delta S = 0$ , the Euler–Lagrange equation for  $A(x, t)$  is obtained

$$\partial_x \left[ \frac{\partial \mathcal{L}}{\partial(\partial_x A^*)} \right] + \partial_t \left[ \frac{\partial \mathcal{L}}{\partial(\partial_t A^*)} \right] - \frac{\partial \mathcal{L}}{\partial A^*} = 0. \tag{4}$$

In this work, we are interested in studying those physical phenomena that may be described by amplitude equations such as the variants of the nonlinear Schrödinger equation or, in general, by the Ginzburg–Landau equation. In this case, the continuous field  $A(x, t)$  is identified as the complex amplitude in those equations and, in general, a suitable Lagrangian density to address those kinds of problems without damping ( $\mu = 0$ ) could be the following:

$$\begin{aligned} \mathcal{L} = & \frac{i}{2}(A\partial_t A^* - A^*\partial_t A) - \sigma|\partial_x A|^2 + i\frac{\eta}{2}(A^{*2} - A^2) \\ & - \frac{\gamma}{2}|A|^4 + |A|^2[\nu - N_0 \sin^2(Kx)]. \end{aligned} \tag{5}$$

Hence, replacing this Lagrangian density in the Euler–Lagrange equation (4), gives the amplitude equation (1) for the  $\mu = 0$  case.

From the Lagrangian density, the corresponding Hamiltonian density can be deduced [68]. In this case, the Hamiltonian density is related to the energy of the system and has the form of

$$\mathcal{H} = \mathcal{P}\partial_t A + \mathcal{P}^*\partial_t A^* - \mathcal{L}, \quad (6)$$

where  $\mathcal{P} = \partial\mathcal{L}/\partial(\partial_t A)$  is the canonical momentum density. Thus, by using Eq. (5), we arrive at

$$\mathcal{H} = \sigma|\partial_x A|^2 - i\frac{\eta}{2}\left(A^{*2} - A^2\right) + \frac{\gamma}{2}|A|^4 - |A|^2[\nu - N_0 \sin^2(Kx)]. \quad (7)$$

We can observe that this equation is not an explicit function of time. Therefore, the energy of the whole system,  $E_\nu$ , will be conserved

$$E_\nu = \int_{-\infty}^{+\infty} \left\{ \sigma|\partial_x A|^2 - i\frac{\eta}{2}\left(A^{*2} - A^2\right) + \frac{\gamma}{2}|A|^4 - |A|^2[\nu - N_0 \sin^2(Kx)] \right\} dx = \text{const.} \quad (8)$$

In this work, we see convenient to establish a global description in terms of ordinary differential equations from the original problem described by partial differential equations. In order to achieve this goal, the variational and moment methods described below allow us to pass from a system of infinite spatial degrees of freedom to one with a finite number of dynamical parameters, which are only related to the intrinsic soliton properties. In this sense, we talk about the spatial nonlocality of this global description.

### 2.3. Nonlocal Lagrangian method

Based on the numerical simulations, we adopt the same Ansatz of Ref. [41] for the space-time profile of a soliton, with the only difference that we exchange the space and time variables to be in accordance with the standard notation of the NLSE

$$A(x, t) = \rho(t) \operatorname{sech} \left[ \frac{x - x_0(t)}{\tau(t)} \right] e^{i(\theta(t) + \omega(t)x)}, \quad (9)$$

where  $\rho(t)$ ,  $\tau(t)$ , and  $x_0(t)$  are the soliton amplitude, mean width, and mean position, respectively; while  $\omega(t)$  and  $\theta(t)$  are their spatial frequency and phase, respectively.

The nonlocality or globality of the method consists in replacing this Ansatz in the Lagrangian density and then integrating it over the whole space. By doing so, we obtain an averaged Lagrangian that is only a function of time

$$L = \int_{-\infty}^{\infty} \mathcal{L} dx = 2\tau\rho^2 \left\{ \dot{\theta} + x_0\dot{\omega} - \sigma\omega^2 - \frac{\sigma}{3\tau^2} - \frac{\gamma\rho^2}{3} + \nu - \frac{N_0}{2} \left[ 1 - \frac{\cos(2Kx_0)}{\operatorname{sinhc}(\pi K\tau)} \right] + \eta \frac{\sin(2[\theta + x_0\omega])}{\operatorname{sinhc}(\pi\omega\tau)} \right\}, \tag{10}$$

where the dot represents the derivative with respect to time and  $\operatorname{sinhc}(\cdot) = \sinh(\cdot)/(\cdot)$ . Using this Lagrangian in the Euler–Lagrange equations,  $\frac{d}{dt} \frac{\partial L}{\partial \xi} - \frac{\partial L}{\partial \xi}$ , where  $\xi = \{\tau, \omega, x_0, \theta, \rho\}$ , we obtain, respectively

$$\frac{1}{\tau} = -\frac{\gamma}{2\sigma}\tau\rho^2 + \frac{3N_0\tau}{4\sigma} \left\{ \operatorname{cothc}(\pi K\tau) - 1 \right\} \frac{\cos(2Kx_0)}{\operatorname{sinhc}(\pi K\tau)} + \frac{3\eta\tau}{2\sigma} \left\{ \operatorname{cothc}(\pi\omega\tau) - 1 \right\} \frac{\sin(2[\theta + x_0\omega])}{\operatorname{sinhc}(\pi\omega\tau)}, \tag{11}$$

$$\dot{x}_0 = -2\sigma\omega - \frac{\eta}{\omega} \left\{ \operatorname{cothc}(\pi\omega\tau) - 1 \right\} \frac{\sin(2[\theta + x_0\omega])}{\operatorname{sinhc}(\pi\omega\tau)}, \tag{12}$$

$$\dot{\omega} = N_0 \frac{K \sin(2Kx_0)}{\operatorname{sinhc}(\pi K\tau)} - 2\eta \frac{\omega \cos(2[\theta + x_0\omega])}{\operatorname{sinhc}(\pi\omega\tau)}, \tag{13}$$

$$\frac{d}{dt} \log(\tau\rho^2) = 2\eta \frac{\cos(2[\theta + x_0\omega])}{\operatorname{sinhc}(\pi\omega\tau)}, \tag{14}$$

$$\begin{aligned} \dot{\theta} = & \frac{1}{2}\gamma\rho^2 + \sigma\omega^2 - \nu + \frac{1}{2}N_0 \\ & - \left\{ N_0 \frac{K \sin(2Kx_0)}{\operatorname{sinhc}(\pi K\tau)} - 2\eta \frac{\omega \cos(2[\theta + x_0\omega])}{\operatorname{sinhc}(\pi\omega\tau)} \right\} x_0 \\ & - \frac{N_0}{4} \{3 - \operatorname{cothc}(\pi K\tau)\} \frac{\cos(2Kx_0)}{\operatorname{sinhc}(\pi K\tau)} \\ & - \frac{\eta}{2} \{3 - \operatorname{cothc}(\pi\omega\tau)\} \frac{\sin(2[\theta + x_0\omega])}{\operatorname{sinhc}(\pi\omega\tau)}, \end{aligned} \tag{15}$$

where  $\operatorname{cothc}(\cdot) = (\cdot)/\tanh(\cdot)$ .

At this point, our model still does not consider dissipative processes. These are taken into account in the method below, and although the dissipative term can formally be obtained from a variational principle, as in

Ref. [69], in this work, we obtain it from the method of moments, which is used mainly to characterize the mean behavior of the numerical solutions found.

#### 2.4. Method of moments

To characterize the solutions of the cubic-FPDDNLSE and to complement the results of the previous method, we use the method of moments. This method is based on constructing a system of equations that allow us to analyze the evolution of the properties of a solitary wave before knowing its explicit form [21]. Each of these properties is assigned to an integral called moment. The lower order ones we consider are

$$\begin{aligned}
 I_1 &= \int_{-\infty}^{\infty} |A|^2 dx, & I_2 &= \frac{1}{2} \int_{-\infty}^{\infty} (A \partial_x A^* - A^* \partial_x A) dx, \\
 D_1 &= \int_{-\infty}^{\infty} x |A|^2 dx, & D_2 &= \int_{-\infty}^{\infty} (x - x_0)^2 |A|^2 dx, \\
 M_1 &= \int_{-\infty}^{\infty} (x - x_0) (A^* \partial_x A - A \partial_x A^*) dx.
 \end{aligned} \tag{16}$$

By using the Ansatz given by Eq. (9), we have that  $I_1 = 2\tau\rho^2 = Q$  measures the area below the curve of the squared  $|A|$  amplitude. Depending on the context, it could be called mass, charge, intensity, energy, power, *etc.* [70].  $iI_2 = \omega I_1 = P$  is called *momentum* associated to the function  $A$  [70], and although its mathematical structure is similar to that of the probability current in quantum mechanics, its interpretation here is different because it is rather related to a phase parameter of the soliton.  $D_1/I_1 = x_0$  represents the coordinate of the *center of mass* of the  $|A|^2$  distribution, giving us an idea of its global position.  $D_2 = \pi^2\tau^2 I_1/12$  is related to the squared width of the  $|A|^2$  pulse, and  $M_1$  is a higher-order moment which is zero for the Ansatz of Eq. (9), and whose interpretation is similar to that of  $D_1$  except that the weight distribution is a probability current density type function instead of a probability density type one. It is noteworthy that among these values, the  $\theta$  phase does not appear, which is because we have considered this parameter only as a function of time.

The equations of system evolution can be obtained by deriving the moments given by Eq. (16) with respect to time. For the integrations, and since we are considering spatially localized solutions, the amplitude  $A$  and its derivatives are considered to be quadratically integrable functions that

cancel out at infinity. In this way, we obtain the set of equations

$$\frac{\dot{I}_1}{2} = \eta \int_{-\infty}^{\infty} \text{Re } A^2 dx - \mu I_1, \tag{17}$$

$$\frac{\dot{I}_2}{2} = -i \frac{N_0}{2} K \int_{-\infty}^{\infty} |A|^2 \sin(2Kx) dx - \mu I_2, \tag{18}$$

$$\frac{\dot{D}_1}{2} = \eta \int_{-\infty}^{\infty} x \text{Re } A^2 dx - i\sigma I_2 - \mu D_1, \tag{19}$$

$$\frac{\dot{D}_2}{2} = \eta \int_{-\infty}^{\infty} (x - x_0)^2 \text{Re } A^2 dx + i\sigma M_1 - \mu D_2, \tag{20}$$

$$\begin{aligned} \frac{\dot{M}_1}{2} = & -2i\sigma \int_{-\infty}^{\infty} |\partial_x A|^2 dx - i \frac{\gamma}{2} \int_{-\infty}^{\infty} |A|^4 dx - \mu M_1 \\ & + iN_0 K \int_{-\infty}^{\infty} (x - x_0) |A|^2 \sin(2Kx) dx + I_2 \dot{x}_0. \end{aligned} \tag{21}$$

Replacing the Ansatz given by Eq. (9) in the preceding equations, we arrive at the same set of Eqs. (11), (12), (13), and (14), except that in the latter, the additional dissipation term  $2\mu$  appears in the form of

$$\frac{d}{dt} \log(\tau \rho^2) = -2\mu + 2\eta \frac{\cos[2(\theta + x_0\omega)]}{\text{sinhc}(\pi\omega\tau)}. \tag{22}$$

The presence of this dissipative term makes the energy  $E_\nu$  no longer constant. Replacing the Ansatz Eq. (9) in Eq. (8), we obtain for  $E_\nu$

$$\begin{aligned} \frac{E_\nu}{2\tau\rho^2} = & \frac{\sigma}{3\tau^2} + \frac{N_0}{2} - \nu + \frac{\gamma\rho^2}{3} + \sigma\omega^2 \\ & - \frac{N_0}{2} \frac{\cos(2Kx_0)}{\text{sinhc}(\pi K\tau)} - \eta \frac{\sin(2[\theta + x_0\omega])}{\text{sinhc}(\pi\omega\tau)}, \end{aligned} \tag{23}$$

which could be useful to follow the energy balance, even in the dissipative case.

In summary, each of the above described methods delivers partial information about the soliton dynamics given by a set of ordinary differential equations. The variational method for conservative systems introduces the

complete set of independent variables and its temporal variation; additionally, the method of moments allows us to introduce dissipative processes at the dynamical level in the system energy balance equation (22). The complementation of these two methods gives us four differential equations (12), (13), (15), and (22), and one constraint equation (11), for the five variables of our Ansatz  $\{\tau, \omega, x_0, \theta, \rho\}$  which will be used to both analyse and characterize the results of the numerical simulations below.

### 3. Results and discussion

We solve numerically Eq. (1) in space and time varying only the amplitudes of the forcing fields,  $\eta$  and  $N_0$ , on the one hand, and varying only their frequencies  $\nu$  and  $K$ , on the other hand. The results of this integration are shown in Figs. 1 and 2. We take as referencing parameter values the following set:  $\mu = 1$ ,  $\eta = 3$ ,  $\nu = -3$ ,  $\sigma = 1$ ,  $\gamma = -1$ ,  $K = 0.2$ , and  $N_0 = 1.5$ . Furthermore, for a more detailed numerical analysis, whose results are shown in Figs. 3 and 4, we use two testing lines within the diagrams of Figs. 1 and 2. Finally, six objects were selected as examples over these lines, whose results are summarized in Figs. 5–10. Clearly, the results observed in all these figures show the existence of regions of chaotic localized structures that coexist alongside regions of null and breather solutions for different ranges of the control parameters, which in this case are the amplitudes and frequencies of the temporal and spatial forcing fields. Moreover, the solutions of the presented theoretical model are shown, which give a trend of the average behavior of the numerical solutions, allowing a qualitative analysis and, to a certain extent, also a quantitative description of the physics involved. Hence, a brief analysis is performed with the aid of the preceding equations.

In Figs. 1 and 2, we show the regions where localized and extended chaotic structures exist for the two sets of chosen ranges of amplitudes and frequencies of the external forcing fields, which are identified by values of the amplitude  $\rho$  other than zero in panels (a) of these figures. What we can see from these diagrams is that no structure is found for relatively large (small) amplitudes of the spatial (temporal) field, which can be interpreted as that the small disturbances promoted by the temporal field are completely smashed by the intense space field in these regions. Besides, there are no structures for relatively low (high) spatial (temporal) frequencies, which can be interpreted by saying that the increase in the frequency of the spatial field counteracts the destructive effect due to rapidly oscillating temporal fields. Note that in all cases, the height of the profiles obtained are of the same order, between  $\rho \simeq 3$  and  $\rho \simeq 4$ .

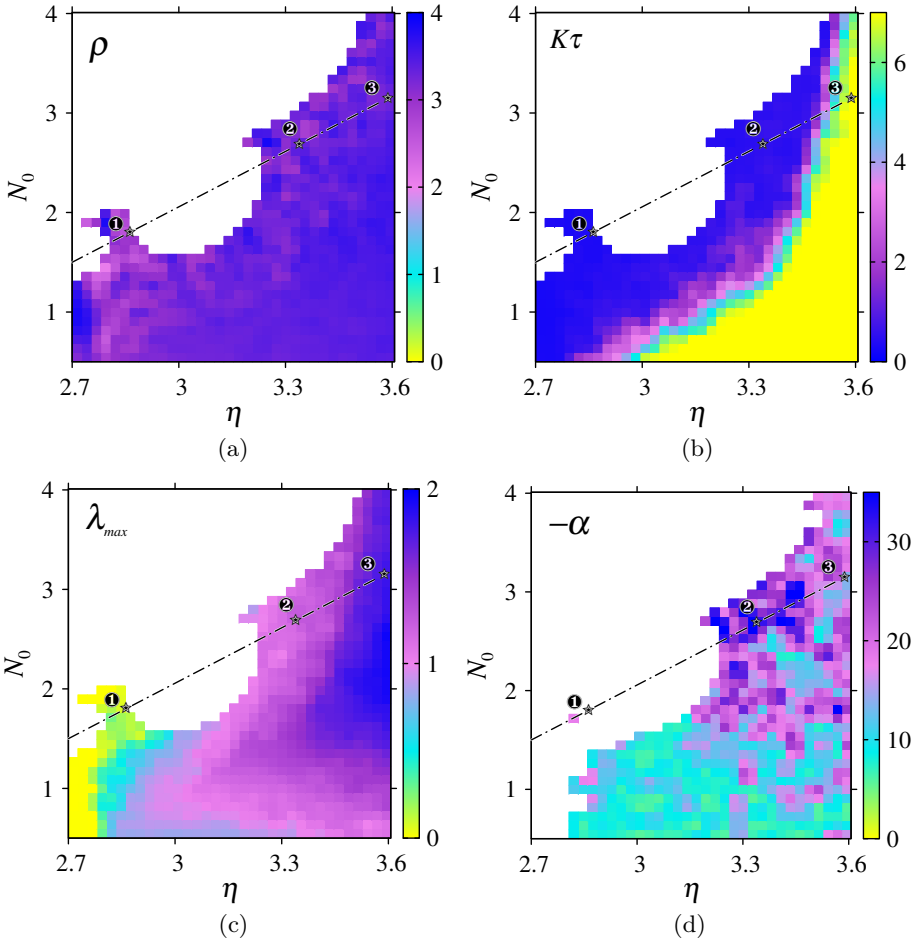


Fig. 1. Diagrams for the soliton amplitude,  $\rho$ , the soliton or soliton cluster width,  $\tau$  (in  $K^{-1}$  units), the largest Lyapunov exponent,  $\lambda_{max}$ , and the fractal exponent  $\alpha$  in the case of  $\mu = 1$ ,  $\sigma = 1$ ,  $\gamma = -1$ , and for the forcing amplitudes scanning with fixed frequencies  $\nu = -3$  and  $K = 0.2$ . Dash-dotted lines represent test lines to study in more detail the characteristic magnitudes in Fig. 3. Over each of those lines, three objects were selected, whose spatio-temporal behavior, energy, phase diagrams, and spectral distributions are shown in Figs. 5 and 8. These results were obtained numerically for the range of  $t \in [0, 400]$ .

As a next step, we analyze the product  $K\tau$ , which gives us an estimation of the soliton or solitons cluster width,  $\tau$ , in units of the minimum distance between peaks of the spatial field,  $K^{-1}$ . Corresponding results are shown in panels (b) of Figs. 1 and 2, where the relative width  $K\tau$  is mapped. What we can see in these panels is that the maps are dominated by structures that are constricted between only two contiguous peaks of the spatial potential,

those for which  $K\tau \leq 1$ , and that the structures become more extended (with greater widths) for greater values of the intensity of the temporal field,  $\eta$ .

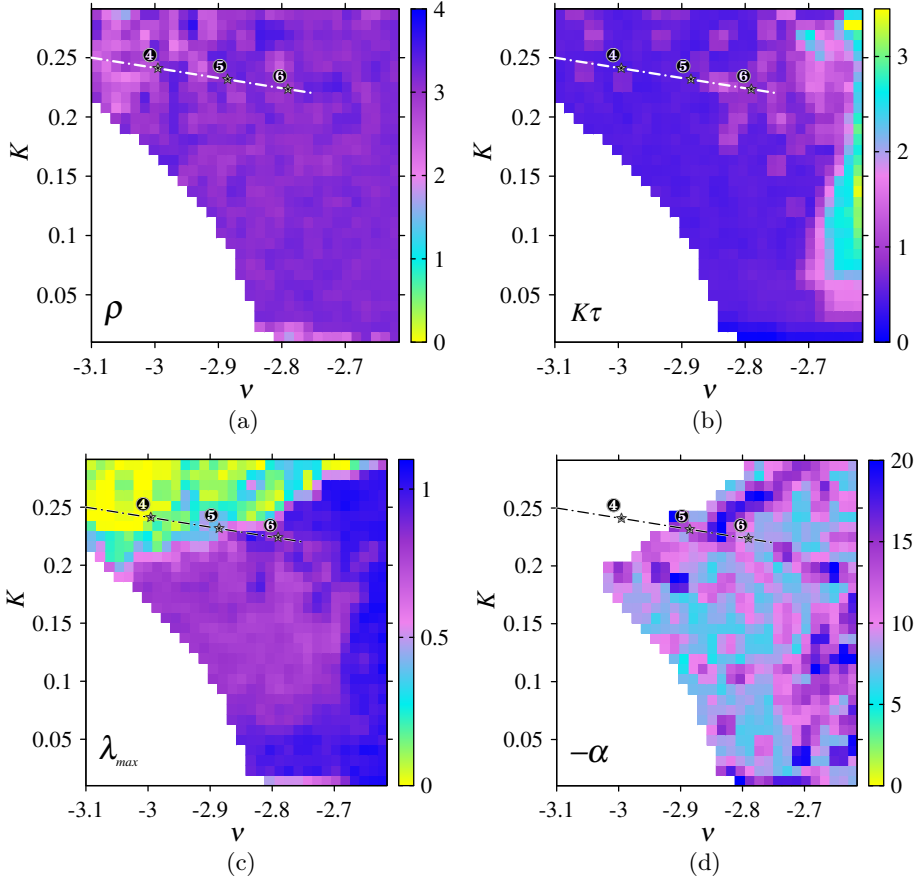


Fig. 2. *Idem* Fig. 1 but for the forcing fields frequencies scanning with fixed amplitudes  $\eta = 3$  and  $N_0 = 1.5$ .

In order to characterize the chaotic content of these structures, the largest Lyapunov exponent ( $\lambda_{\max}$ ) is numerically obtained for each one. The  $\lambda_{\max}$  calculation is made as in Refs. [44, 71], solving additionally the equation that comes from performing a virtual variation of the complex amplitude in Eq. (1)

$$i\partial_t\delta A - \sigma\partial_x^2\delta A + \gamma(2|A|^2\delta A + A^2\delta A^*) = (\nu - i\mu)\delta A + i\eta\delta A^* - N_0\sin^2(Kx)\delta A, \quad (24)$$

where  $\delta A$  is the fluctuation in the amplitude of two paths initially very close to each other. By defining the average “distance” between these paths as  $d(t) = \sqrt{\int |\delta A|^2 dx}$ , and knowing that for the chaotic case this length tends to increase exponentially fast, we rescale  $\delta A$  as  $\delta A d(t_0)/d(t)$  after every step  $\Delta t$  to the initial length at  $t_0$ . Therefore, the largest Lyapunov exponent is obtained as an average from the expression  $\lambda_{\max} = \lim_{M \rightarrow \infty} \frac{1}{M} \sum_{i=1}^M \log[d(t_0 + M\Delta t)/d(t_0)]/M\Delta t$ . Thus, a positive value of  $\lambda_{\max}$  indicates that the structure under study is chaotic, in the sense that two initially very close paths are quickly separated, exponentially, at the rate given by  $\lambda_{\max}$ . Results for  $\lambda_{\max}$  are shown in panels (c) of Figs. 1 and 2. What we can see in these panels is that all the structures obtained are chaotic, and that they are more chaotic for higher values of the amplitudes of the space-time fields,  $N_0$  and  $\eta$ , as well as for lower values of the frequencies of these fields,  $K$  and  $|\nu|$ , respectively.

In addition, in order to characterize the behavior of the objects found in the space of frequencies,  $\varpi$ , we consider the spectral distribution  $N(s)$  defined as the number of peaks with heights greater than  $s$  of the normalized Fourier power spectrum,  $|S(\varpi)|/|S(\varpi)|_{\max}$  [72]. What we have found is that all chaotic objects have a spectral distribution that obeys the form  $\log N(s) = \alpha s + b_0$ , with relatively high values of the spectral index  $-\alpha$ , as shown in panels (d) of Figs. 1 and 2. However, due to an insufficient number of peaks,  $\alpha$  is not statistically obtainable for objects with very low positive values of the largest Lyapunov exponent, as can be seen in Figs. 1 and 2.

In Figs. 3 and 4, the results of some characteristic magnitudes for the structures on the dash-dotted test lines specified in Figs. 1 and 2 are shown, all this once the transient state is far overcome at  $t = 400$ . What can be observed in these figures is that by increasing (decreasing) the intensity (the frequency module) of the temporal field on those lines, the chaotic content of the structures also increases: they become more widespread and with a greater maximum Lyapunov exponent. In turn, the values of the spectral index  $-\alpha$  become obtainable with low scattering, while the maximum and minimum of energy and momentum become increasingly scattered and disordered.

For the example objects indicated in Figs. 1 and 2, we solve numerically the set of model global equations (11), (12), (13), (15), (22), (23), and compare (Figs. 5–10) the results with the corresponding data of the direct spatio-temporal integration and with the averages made on them via the moments method. All this in order to assess to what extent the nonlocal equations can give us a precise and enough quantitative image of the objects studied in this manuscript. As expected, the model given by the Ansatz of

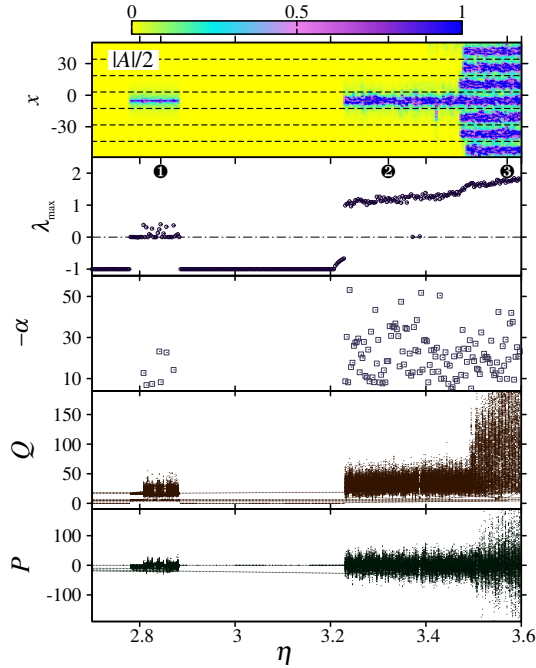


Fig. 3. Characteristic magnitudes for the sampling line of equation  $N_0(\eta) = 13[\eta - 2.7]/7 + 1.5$  for  $\nu = -3$  and  $K = 0.2$  (shown in Fig. 1). From up to down: maps of  $|A|$  at  $t = 400$ , where the dashed lines represent the maxima of the periodic spatial field of amplitude  $N_0$ ; the largest Lyapunov exponent,  $\lambda_{\max}$ ; spectral index  $-\alpha$  (if calculable); and bifurcation diagrams made with the extrema values (maxima and minima) of the energy,  $Q = 2\tau\rho^2$ , and momentum,  $P = \omega Q$ . The three examples selected in Fig. 1 are also indicated.

Eq. (9) represents a kind of ultimate average with respect to the numerical results, reaching stationary values for the parameters of the model within the ranges of the corresponding numerical values obtained. Note that, examining the confined objects in Figs. 5–10, they can be seen as molecules of two or more simple solitons that seem to interact with each other in an intricate way. Moreover, in some cases, quasiperiodic-like chaotic objects coexist with highly chaotic ones, as in the case of the breather shown in Fig. 8.

Figures 5–10 show the results for the six structures chosen on the test lines indicated in figures 1–4. These objects were selected in order to perform a more detailed analysis on the behavior of the structures that appear for different values of the control parameters. To carry out this task, we will resort to the equations of the global model described in previous sections. Then, for a qualitative analysis of the numerical results, we consider, as a convenient approach, the stationary state, which is reached numerically

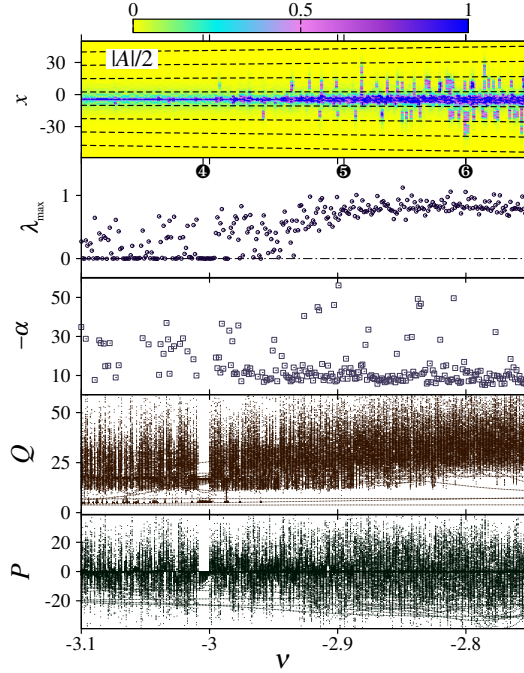


Fig. 4. *Idem* Fig. 3 but for the sampling line of equation  $K(\nu) = -3[\nu + 3.1]/35 + 0.25$  for  $\eta = 3$  and  $N_0 = 1.5$  (shown in Fig. 2).

for enough large times. In this case, Eq. (12) turns into  $\dot{x}_0 = 0$ , indicating that the momentum  $\omega = 0$  and that the soliton bulk position is static. This approach works well by observing that it matches the results of the model in panels (c) of Figs. 5–10, once the initial relaxation process has been passed, where  $\omega = 0$  and  $x_0$  has a fixed value in the middle of two maxima of the spatial field, which can be explained considering that Eq. (13) becomes

$$0 = \dot{\omega} = N_0 \frac{K \sin(2Kx_0)}{\operatorname{sinhc}(\pi K\tau)}, \tag{25}$$

with zeros:  $2Kx_0 = m\pi$ ,  $m = 0, \pm 1, \pm 2, \dots$ . Hence, in the stationary case, the object is centered in a maximum of the spatial field for  $m$  odd, and in between two adjacent maxima of the same field for  $m$  even, which is our case for  $\sigma > 0$  and  $\gamma < 0$ . We can see that this effect also takes place for the structures shown in the space-time maps of Figs. 3, 4, and panels (a) of Figs. 5–10, as well as for the phase coordinates shown in panels (c) of Figs. 5–10, except for the moments average when the structures extend beyond the initial potential well. This localization within the wells of the spatial potential is what we recognize as soliton confinement.

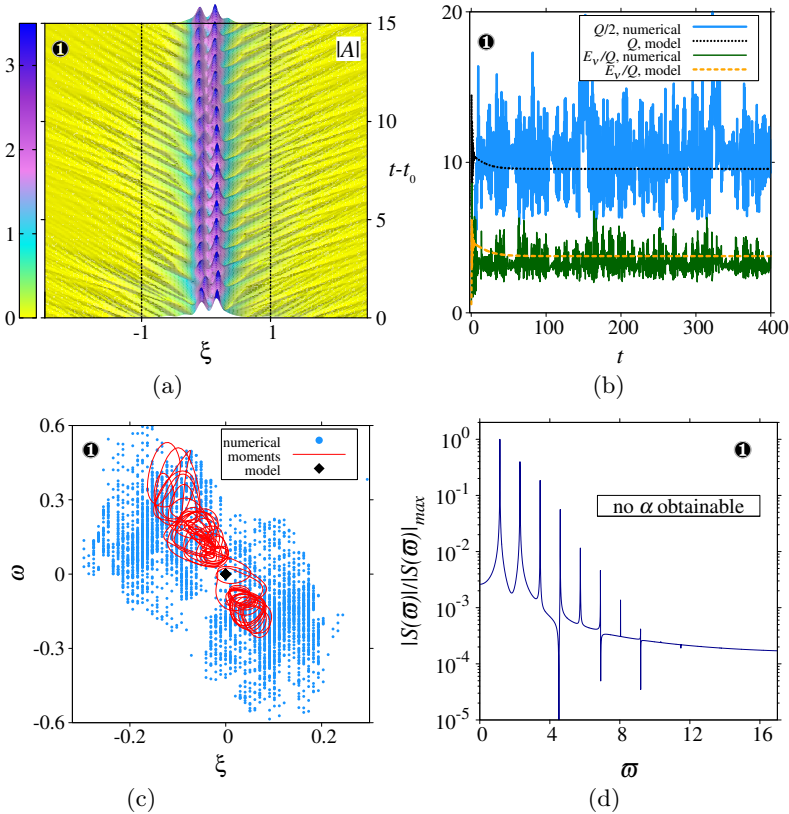


Fig. 5. Dynamical results for object **1** of Fig. 1, with parameters  $\{\eta; N_0\} = \{2.844; 1.767\}$  and  $\lambda_{\max} = 0.075$ . Integrations were made from  $t = 0$  to  $t = 400$  starting from a displaced sech-like arbitrary initial condition. Dashed lines represent the maxima of the spatial periodic field. Panel (a) shows the amplitude module spatio-temporal maps (where  $t_0 = 385$  and  $\xi = 2Kx/\pi$ ). Panel (b) shows the energy per single soliton,  $Q/n$  (where  $n$  is the estimated number of single solitons for the whole structure), and the system energy per total object energy,  $E_\nu/Q$  (Eq. (23)). Panel (c) shows phase sections for  $t \in [350, 400]$  and for three cases: Numerical, where the phase points of soliton peaks are shown as dots, being  $\xi = 2Kx_{\text{peaks}}/\pi$  its normalized position. Moments, where the continuous lines are obtained by applying the moment averages over numerical data, being  $\xi = 2KD_1/I_1\pi$ . Model, where the only one point is obtained by integrating the ordinary differential equations system that comes from the Ansatz, Eq. (9), being in this case  $\xi = 2Kx_0/\pi$ . Finally, in panel (d), the corresponding Fourier power spectrum  $|S(\omega)|/|S(\omega)|_{\max}$  and the spectral distribution  $N(s)$  (if obtainable) are plotted.

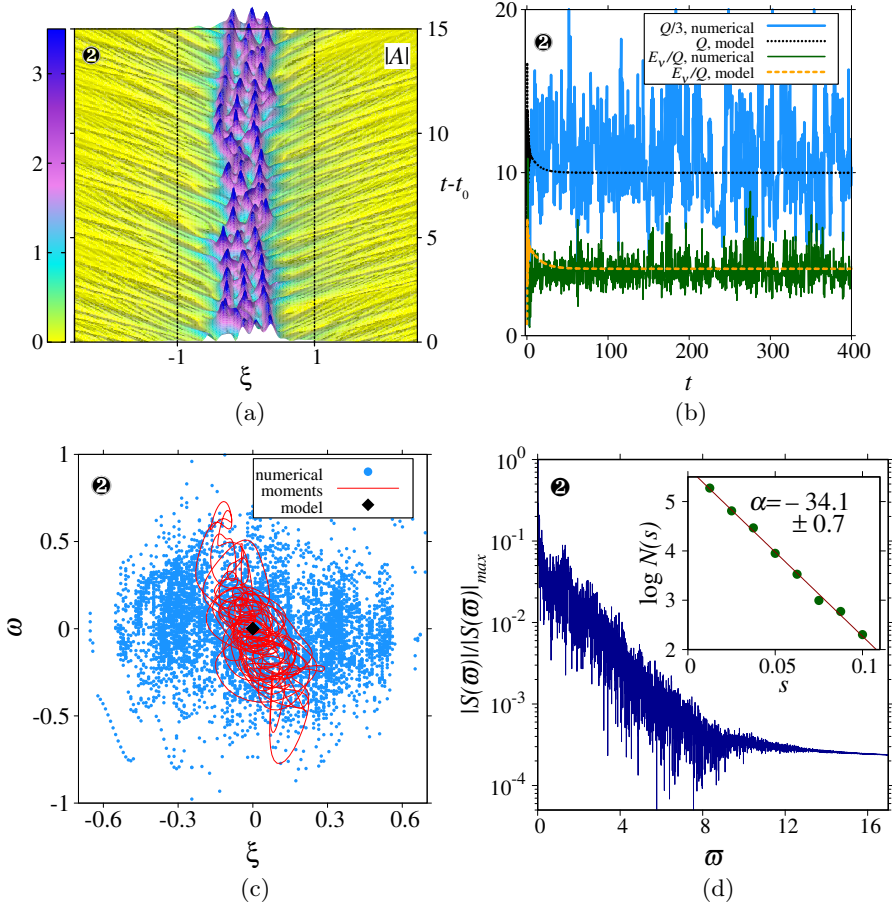


Fig. 6. *Idem* Fig. 5 but for object ② of Fig. 1, with parameters  $\{\eta; N_0\} = \{3.321; 2.653\}$  and  $\lambda_{\max} = 1.107$ .

At the same time, Eq. (22) for  $\omega = 0$  is reduced to

$$0 = \frac{d}{dt} \log(\tau \rho^2) = \frac{d}{dt} \log Q = 2[-\mu + \eta \cos(2\theta)] , \tag{26}$$

which means that the soliton energy rate of change is governed by the competition between the injected energy by the temporal field of amplitude  $\eta$  and the dissipated energy at the rate given by its coefficient  $\mu$ , as seen in Fig. 3, for increasing or decreasing  $\eta$ . When the former dominates, the object expands, being divided into pieces that are further trapped in adjacent wells of the spatial field. On the other hand, when the latter dominates, soliton energy  $Q$  is completely dissipated and the object disappears. In the case of equilibrium, there is an exact energy balance between these two effects and the phase  $\theta$  becomes stationary with the value  $\cos(2\theta) = \mu/\eta$ ,

which is the case exemplified in the results of the model shown in panels (b) of Figs. 5–10. In this case, the integration of the ordinary differential equations of the theoretical model informs us that the system reaches this state of energetic equilibrium after having overcome the relaxation process. Therefore, we emphasize that, to support stable and stationary solitons, the role of temporal periodic driving is necessary when damping is considered [65].

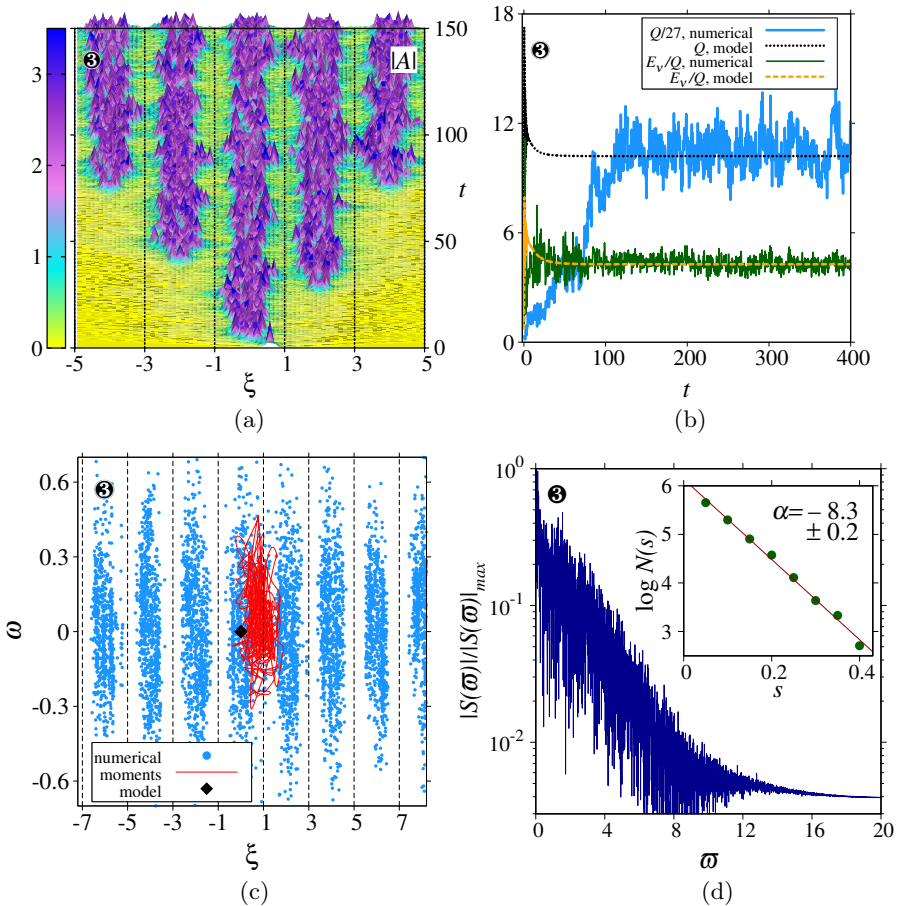


Fig. 7. *Idem* Fig. 5 but for object 3 of Fig. 1, with parameters  $\{\eta; N_0\} = \{3.570; 3.116\}$  and  $\lambda_{\max} = 1.667$ .

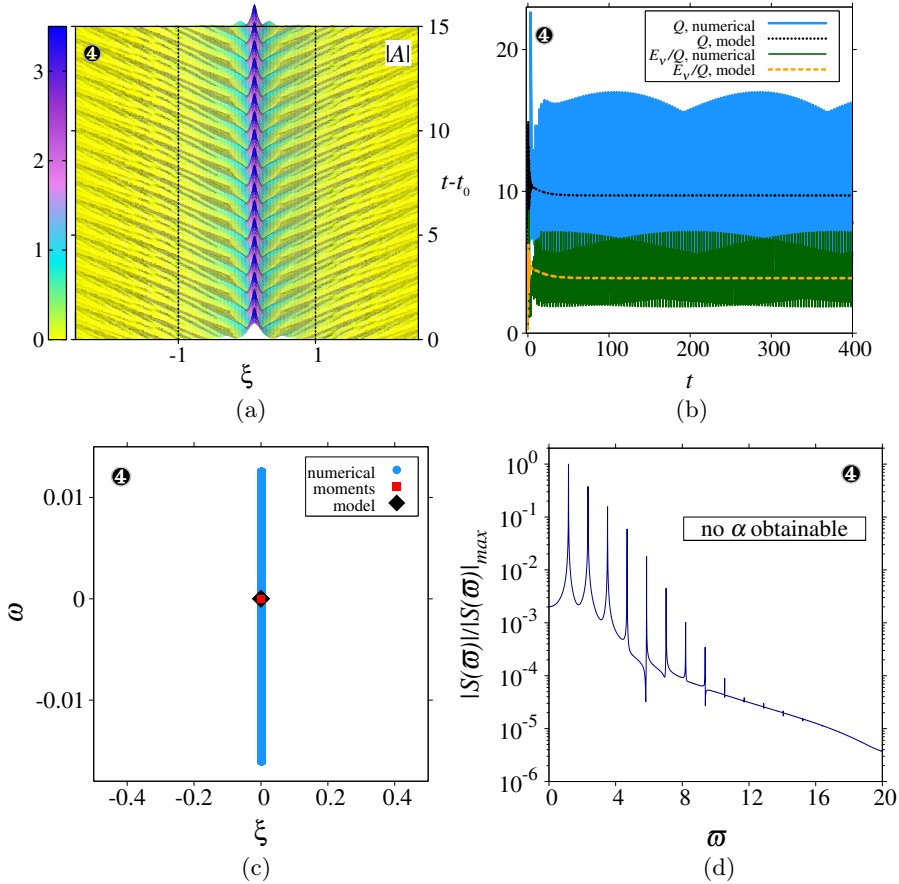


Fig. 8. *Idem* Fig. 5 but for object 4 of Fig. 2, with parameters  $\{\nu; K\} = \{-3.005; 0.242\}$  and  $\lambda_{\max} = 0.009$ .

Following this approach, and for  $m$  even, Eqs. (15), (11), and (23) take the forms of

$$0 = \dot{\theta} = \frac{N_0}{2} \left[ 1 - \frac{3 - \operatorname{cothc}(\pi K \tau)}{2 \operatorname{sinhc}(\pi K \tau)} \right] + \frac{\gamma \rho^2}{2} - \nu - \eta \sin(2\theta), \quad (27)$$

$$\tau^2 = \frac{\sigma}{-\frac{\gamma \rho^2}{2} + \frac{3N_0}{4} \frac{\operatorname{cothc}(\pi K \tau) - 1}{\operatorname{sinhc}(\pi K \tau)}} \quad (28)$$

and

$$\frac{E_\nu}{Q} = \frac{N_0}{2} \left[ 1 - \frac{1}{\operatorname{sinhc}(\pi K \tau)} \right] + \frac{\sigma}{3\tau^2} + \frac{\gamma \rho^2}{3} - \nu - \eta \sin(2\theta). \quad (29)$$

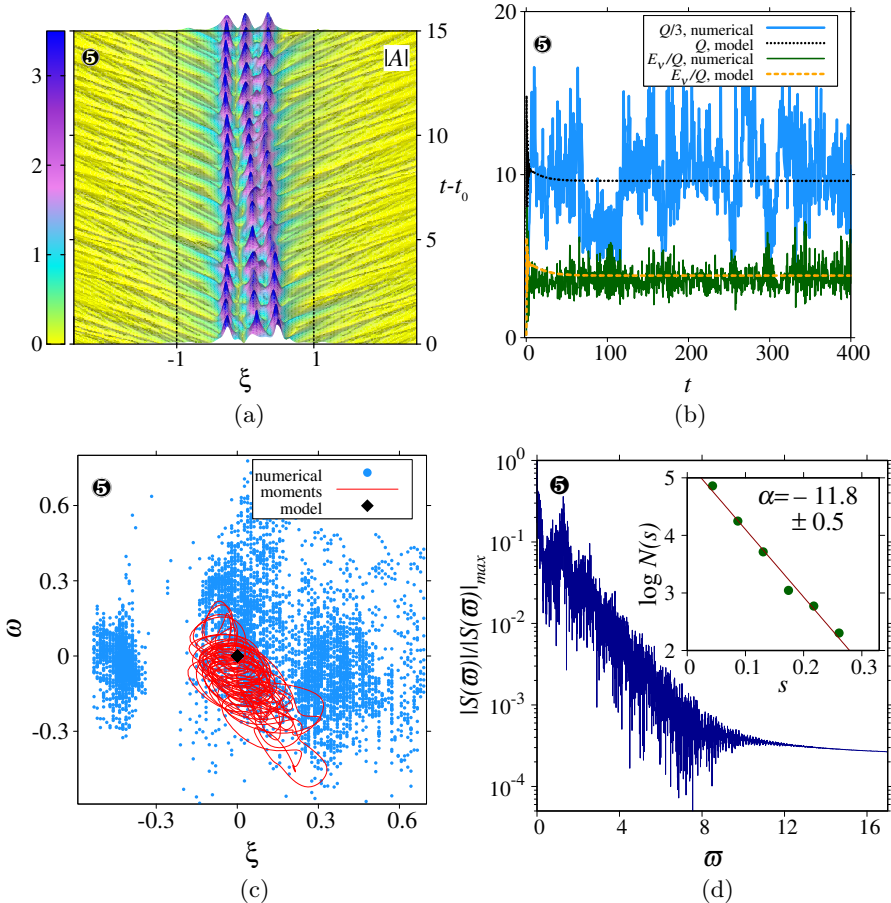


Fig. 9. *Idem* Fig. 5 but for object 5 of Fig. 2, with parameters  $\{\nu; K\} = \{-2.895; 0.232\}$  and  $\lambda_{\max} = 0.645$ .

Equation (27) tells us that in the stationary regime, the soliton amplitude is given by

$$\rho = \sqrt{\frac{2}{\gamma} \left( \nu + \eta \sin(2\theta) - \frac{N_0}{2} \left[ 1 - \frac{3 - \operatorname{cothc}(\pi K \tau)}{2 \operatorname{sinhc}(\pi K \tau)} \right] \right)}, \quad (30)$$

being  $\cos(2\theta) = \mu/\eta$  as explained above, which for  $N_0 = 0$  is a well-known solution [5, 65] that demands  $\nu < 0$  in order to have a stable soliton. Replacing Eq. (30) into Eqs. (28) and (29), we obtain, respectively, a transcendental equation for  $\tau$  and the asymptotic values of the system energy per total object energy,  $E_\nu/Q$ , shown in panels (b) of Figs. 5–10.

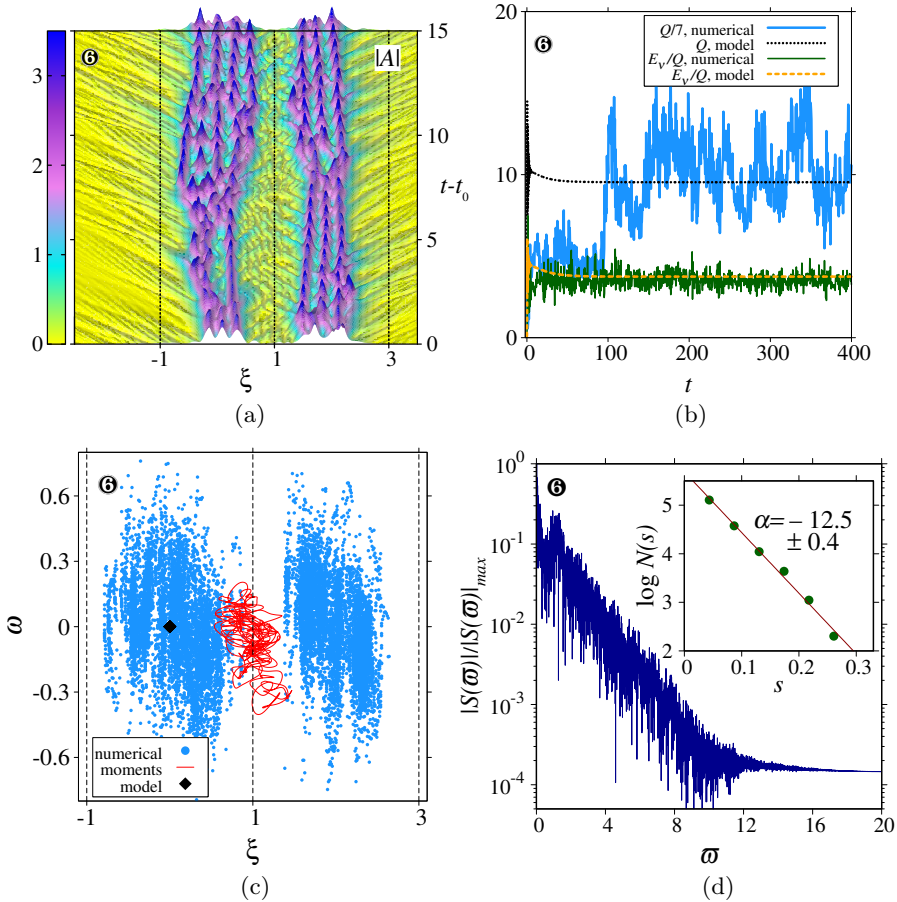


Fig. 10. *Idem* Fig. 5 but for object 6 of Fig. 2, with parameters  $\{\nu; K\} = \{-2.800; 0.224\}$  and  $\lambda_{\max} = 0.921$ .

According to numerical simulations given in Ref. [5] for  $N_0 = 0$ , if  $\eta$  grows to larger positive values, soliton amplitudes begin to be quasiperiodic functions of time, in which case we have a typical breather-soliton behavior. For still larger values of  $\eta$ , we have the formation of expanding chaotic extended domains, for which the soliton model is no longer valid. For  $N_0 > 0$ , the system is never stationary, and rather triggers the chaotic and confined behavior of the soliton that we observe in the simulations as long as  $\eta > 0$ . In this sense, we could talk about a sort of interplay of the external both temporal driving field and spatial periodic potential: The former supports the existence of the soliton against the damping, while the latter originates its confinement and chaotic behavior, according to the previous analysis and Eqs. (26) and (25), respectively. To emphasize this effect, in Fig. 11, we show the spatio-temporal diagram of a structure obtained for the same

set of parameters and for the same initial condition at  $t = 0$  for object **1** in Fig. 5, except that until  $t = 70$ , we deactivate the field taking  $N_0 = 0$ . From this moment forward, the field is activated at its original value and the confinement effect takes place a short interval later, inhibiting the expansion of the preceding chaotic domain.

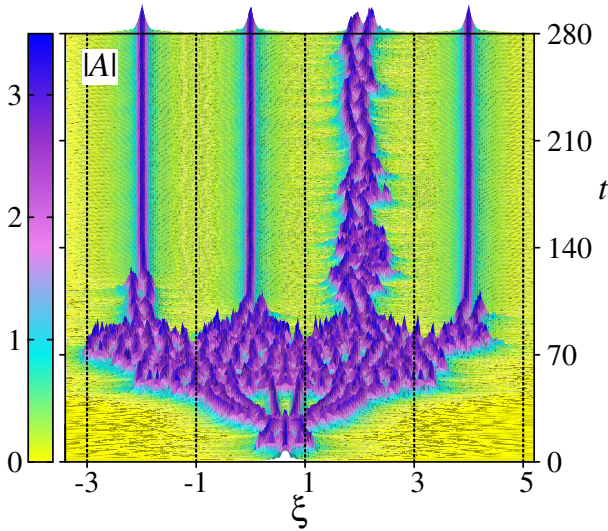


Fig. 11. Spatio-temporal map corresponding to the same parameters and initial condition of object **1** of Fig. 5 unlike the external spatial field is turned on only from  $t = 70$ . The dashed lines represent the maxima of this field and  $\xi = 2Kx/\pi$ .

Panels (d) of Figs. 5–10 show typical Fourier spectra corresponding to the six objects selected as examples. Objects **1** and **4**, chaotic but with low Lyapunov exponents, show quasiperiodic-like spectra, such as those of breathers [5]. In these cases, the number of peaks is insufficient to calculate the  $-\alpha$  spectral index. By contrast, for objects **2**, **3**, **5** and **6**, with high values of the Lyapunov exponent, the spectra have a very high peak density; whose heights are uneven and sparse. The high number of peaks in these cases allows the precise calculation of  $\alpha$ . According to the results found in this work,  $-\alpha$  values are relatively high in all cases for chaotic objects, varying from  $\sim 10$  to  $\sim 50$ .

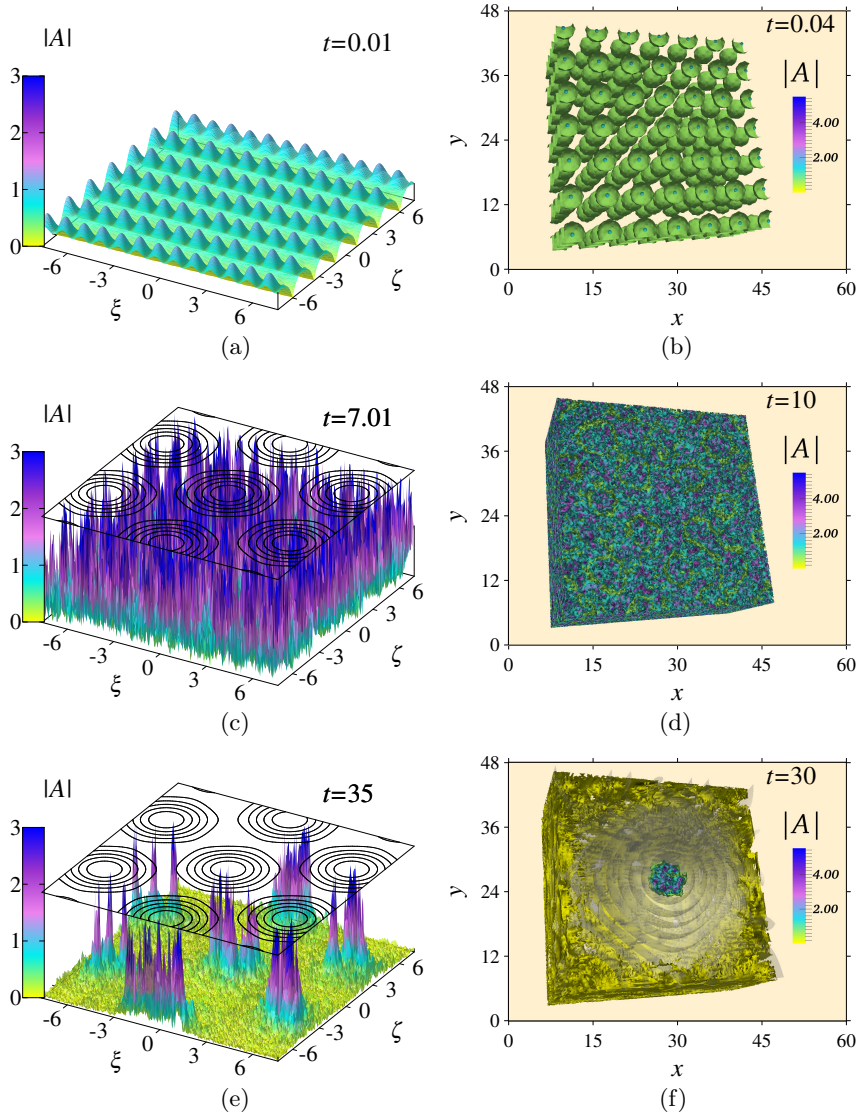


Fig. 12. An example of the chaos confinement effect in two (three) dimensions (where  $\xi = Kx/\pi$  and  $\zeta = Ky/\pi$ ) when the spatial field, given by Eqs. (31), (32), is turned on at  $t = 5$  (10) and is represented by the solid line isosamples (by the isosurfaces in panel (f)). (a), (b): the initial disturbance. (c), (d): the chaotic pattern a little after (just before) the field is turned on. (e), (f): the final state with chaotic 2D solitons (with a chaotic 3D soliton) confined within the valleys (within the hole) of the space field. The complete animations are given in online resources 1 and 2 (see footnote 1).

Finally, the confinement effects of chaotic solitons in 2D and 3D have been investigated. For this purpose, we have used for the 2D case, a space field of hexagonal type given by [73]

$$U_{2D}(x, y) = \frac{2}{9}N_0 \left\{ 3 - \cos \left( K2^{-1} \left( x - y\sqrt{3} \right) \right) - \cos \left( K2^{-1} \left( x + y\sqrt{3} \right) \right) - \cos(Kx) \right\}, \quad (31)$$

and for the 3D case, this potential has been used to build the corresponding 3D potential as follows:

$$U_{3D}(x, y, z) = \frac{1}{2.74} [U_{2D}(x, y) + U_{2D}(y, z) + U_{2D}(z, x)]. \quad (32)$$

Hence, the equation to solve in these cases is modified by adding the corresponding Laplacian terms in  $y$  and  $z$  ( $\partial_x^2 \rightarrow (\partial_x^2 + \partial_y^2)/2$  for the 2D case, and  $\partial_x^2 \rightarrow (\partial_x^2 + \partial_y^2 + \partial_z^2)/3$  for the 3D case), and replacing in Eq. (1)  $U(x) = N_0 \sin^2(Kx)$  by the above fields  $U_{2D}(x, y)$  and  $U_{3D}(x, y, z)$ , respectively.

For parameter values  $\mu = 1$ ,  $\nu = -3$ ,  $\sigma = 1$ , and  $\gamma = -1$ , Fig. 12 shows the results for an example in the 2D (3D) case, with field parameters  $\eta = 2.8$  ( $\eta = 3.0$ ),  $K = 0.4$  ( $K = 0.2$ ), and  $N_0 = 3$  ( $N_0 = 15$ ). Starting from an initial periodic perturbation at  $t = 0$ , a chaotic pattern is rapidly formed in the plane (space). At  $t = 5$  ( $t = 10$ ), the space field is activated and the process of chaos confinement begins, which can be observed as already established in panels (e) and (f) of this figure. The largest Lyapunov exponent at this stage is  $\lambda_{\max} \simeq 10$  ( $\lambda_{\max} \simeq 7$ ). Movies of these simulations are provided as supplementary materials in online resources 1 and 2<sup>1</sup>.

#### 4. Concluding remarks

In summary, we have proposed a model of confinement of chaotic solitons by adding a spatially periodic external field to the cubic order parametrically-driven and damped nonlinear Schrödinger amplitude equation. In the absence of this term, the increase in the intensity of the parametric forcing would have caused a stationary soliton to pass to the breather stage and, subsequently, to the expanding chaotic extended pattern state. Thanks to the new forcing introduced, the pattern is confined between two of its adjacent maxima, or if the intensity of that parametric forcing is sufficiently high, the pattern is divided into pieces, each confined between the maxima of the spatial field and preserving its localized and chaotic character.

<sup>1</sup> Resource 1: [https://www.actaphys.uj.edu.pl/store/appdx/v51p2159\\_1.mp4](https://www.actaphys.uj.edu.pl/store/appdx/v51p2159_1.mp4),  
Resource 2: [https://www.actaphys.uj.edu.pl/store/appdx/v51p2159\\_2.mp4](https://www.actaphys.uj.edu.pl/store/appdx/v51p2159_2.mp4)

To characterize these objects, we have used numerical simulations in 1+1 dimensions, with which we have calculated different typical magnitudes such as the maximum exponents of Lyapunov, widths, heights, momentums, energies, spectral indexes, *etc.* In this way, we have obtained not only the existence diagrams of these objects together with the null and breathers solutions but also their corresponding bifurcation diagrams in different regions of interest.

To complement the analysis, suitable theoretical methods have been used, such as the Lagrangian and Hamiltonian variational methods. The method of moments is also used to correct the equations of the preceding methods in order to consider dissipative processes and to generate the link, via the moments, between theory and simulations. These methods allow us to perform the analysis and discussion of the numerical results, finding a very good agreement between theoretical models and simulations, being the model a kind of average of the numerical results.

Finally, simulations in 1 + 2 and 1 + 3 dimensions were performed to confirm that the confinement effect of chaos also occurs when fields are present in two and three spatial dimensions.

The contribution offered to this work by G.F.M.-F. was his research project to graduate as a physicist, that is why he wants to thank the Universidad Mayor de San Andrés (UMSA), and his teachers and colleagues.

## REFERENCES

- [1] M.G. Clerc, S. Coulibaly, D. Laroze, «Parametrically Driven Instability in Quasi-reversal Systems», *Int. J. Bifur. Chaos* **19**, 3525 (2009).
- [2] G. Theocharis, P. Schmelcher, P.G. Kevrekidis, D.J. Frantzeskakis, «Matter-wave solitons of collisionally inhomogeneous condensates», *Phys. Rev. A* **72**, 033614 (2005).
- [3] A. Gammal, L. Tomio, T. Frederico, «Critical numbers of attractive Bose–Einstein condensed atoms in asymmetric traps», *Phys. Rev. A* **66**, 043619 (2002).
- [4] M.G. Clerc, S. Coulibaly, D. Laroze, «Localized states and non-variational Ising–Bloch transition of a parametrically driven easy-plane ferromagnetic wire», *Physica D* **239**, 72 (2010).
- [5] D. Urzagasti, D. Laroze, M.G. Clerc, H. Pleiner, «Breather soliton solutions in a parametrically driven magnetic wire», *Europhys. Lett.* **104**, 40001 (2013).
- [6] S. Yanez-Pagans, D. Urzagasti, Z. Oporto, «Parametrically driven scalar field in an expanding background», *Phys. Rev. D* **96**, 083503 (2017).

- [7] B.A. Malomed, D. Mihalache, F. Wise, L. Torner, «Spatiotemporal optical solitons», *J. Opt. B: Quantum Semiclass. Opt.* **7**, R53 (2005).
- [8] F. Lederer *et al.*, «Discrete solitons in optics», *Phys. Rep.* **463**, 1 (2008).
- [9] A. Komarov, K. Komarov, A. Niang, F. Sanchez, «Nature of soliton interaction in fiber lasers with continuous external optical injection», *Phys. Rev. A* **89**, 013833 (2014).
- [10] A. Komarov, F. Sanchez, «Structural dissipative solitons in passive mode-locked fiber lasers», *Phys. Rev. E* **77**, 066201 (2008).
- [11] H. Leblond, B.A. Malomed, D. Mihalache, «Interactions of spatiotemporal solitons and vortices in fiber bundles», *Phys. Rev. A* **79**, 033841 (2009).
- [12] D. Mihalache, D. Mazilu, F. Lederer, Y.S. Kivshar, «Spatiotemporal surface Ginzburg–Landau solitons», *Phys. Rev. A* **77**, 043828 (2008).
- [13] Y. Sun, B. Tian, L. Liu, X.Y. Wu, «Rogue waves for a generalized nonlinear Schrödinger equation with distributed coefficients in a monomode optical fiber», *Chaos Solitons Fractals* **107**, 266 (2018).
- [14] K.V. Samokhin, «Helical states and solitons in noncentrosymmetric superconductors», *Phys. Rev. B* **89**, 094503 (2014).
- [15] A.R. Osborne, M. Onorato, M. Serio, «The nonlinear dynamics of rogue waves and holes in deep-water gravity wave trains», *Phys. Lett. A* **275**, 386 (2000).
- [16] M. Onorato, D. Proment, A. Toffoli, «Triggering Rogue Waves in Opposing Currents», *Phys. Rev. Lett.* **107**, 184502 (2011).
- [17] A. Ankiewicz, Y. Wang, S. Wabnitz, N. Akhmediev, «Extended nonlinear Schrödinger equation with higher-order odd and even terms and its rogue wave solutions», *Phys. Rev. E* **89**, 012907 (2014).
- [18] J. Lin, B. Ren, H.m. Li, Y.s. Li, «Soliton solutions for two nonlinear partial differential equations using a Darboux transformation of the Lax pairs», *Phys. Rev. E* **77**, 036605 (2008).
- [19] N.R. Quintero, F.G. Mertens, A. Efimov, A.R. Bishop, «Soliton dynamics in optical fibers using the generalized traveling-wave method», *Phys. Rev. E* **93**, 042214 (2016).
- [20] S. Chakraborty, S. Nandy, A. Barhakur, «Bilinearization of the generalized coupled nonlinear Schrödinger equation with variable coefficients and gain and dark–bright pair soliton solutions», *Phys. Rev. E* **91**, 023210 (2015).
- [21] A.I. Maïmistov, «Evolution of solitary waves which are approximately solitons of a nonlinear Schrödinger equation», *Zh. Eksp. Teor. Fiz.* **104**, 3620 (1993).
- [22] A.B. Nassar, «New method for the solution of the logarithmic nonlinear Schrödinger equation via stochastic mechanics», *Phys. Rev. A* **33**, 3502 (1986).
- [23] V.L. Ginzburg, L.D. Landau, «On the theory of superconductivity», *J. Exp. Theor. Phys. (USSR)* **20**, 1064 (1950).

- [24] V.L. Ginzburg, «On the Macroscopic Theory of Superconductivity», *JETP* **2**, 589 (1956).
- [25] A. Ankiewicz, N. Akhmediev (Eds.) «Dissipative Solitons: From Optics to Biology and Medicine», Springer, Berlin 2008.
- [26] I.S. Aranson, L. Kramer, «The world of the complex Ginzburg–Landau equation», *Rev. Mod. Phys.* **74**, 99 (2002).
- [27] Y.V. Kartashov, B.A. Malomed, L. Torner, «Solitons in nonlinear lattices», *Rev. Mod. Phys.* **83**, 247 (2011).
- [28] W. Chang, J.M. Soto-Crespo, P. Vouzas, N. Akhmediev, «Extreme soliton pulsations in dissipative systems», *Phys. Rev. E* **92**, 022926 (2015).
- [29] M.J. Cassidy, «Nonlinearity in quantum theory and closed timelike curves», *Phys. Rev. D* **52**, 5676 (1995).
- [30] A. Klein, F. Krejs, «Nonlinear Schrödinger equation: A testing ground for the quantization of nonlinear waves», *Phys. Rev. D* **13**, 3282 (1976).
- [31] A. Caticha, «Consistency, amplitudes, and probabilities in quantum theory», *Phys. Rev. A* **57**, 1572 (1998).
- [32] H. Ishio, K. Nakamura, «Quantum irregular spectra: An alternative interpretation from the viewpoint of nonlinear dynamics», *Phys. Rev. A* **46**, R2193 (1992).
- [33] D. Urzagasti, A. Aramayo, D. Laroze, «Soliton–antisoliton interaction in a parametrically driven easy-plane magnetic wire», *Phys. Lett. A* **378**, 2614 (2014).
- [34] D. Urzagasti, D. Laroze, H. Pleiner, «Localized chaotic patterns in weakly dissipative systems», *Eur. Phys. J. Spec. Top.* **223**, 141 (2014).
- [35] D. Urzagasti, D. Laroze, H. Pleiner, «Two-dimensional localized chaotic patterns in parametrically driven systems», *Phys. Rev. E* **95**, 052216 (2017).
- [36] J.Y. Lee *et al.*, «Dynamic transformations of the internal structure of a moving domain wall in magnetic nanostripes», *Phys. Rev. B* **76**, 184408 (2007).
- [37] A.D. Martin, C.S. Adams, S.A. Gardiner, «Bright solitary-matter-wave collisions in a harmonic trap: Regimes of solitonlike behavior», *Phys. Rev. A* **77**, 013620 (2008).
- [38] D. Turaev, M. Radziunas, A.G. Vladimirov, «Chaotic soliton walk in periodically modulated media», *Phys. Rev. E* **77**, 065201 (2008).
- [39] J. Fujioka *et al.*, «Chaotic solitons in the quadratic–cubic nonlinear Schrödinger equation under nonlinearity management», *Chaos* **21**, 033120 (2011).
- [40] D. Cai, D.W. McLaughlin, J. Shatah, «Spatiotemporal chaos and effective stochastic dynamics for a near-integrable nonlinear system», *Phys. Lett. A* **253**, 280 (1999).
- [41] C.J. Castro, D. Urzagasti, «Seesaw drift of bright solitons of the nonlinear Schrödinger equation with a periodic potential», *J. Nonlinear Opt. Phys. Mater.* **25**, 1650038 (2016).

- [42] D.E. Pelinovsky, A.A. Sukhorukov, Y.S. Kivshar, «Bifurcations and stability of gap solitons in periodic potentials», *Phys. Rev. E* **70**, 036618 (2004).
- [43] C.P. Jisha, A. Alberucci, G. Assanto, « $\mathcal{PT}$ -symmetric nonlocal gap solitons in optical lattices», *J. Nonlinear Opt. Phys. Mater.* **23**, 1450041 (2014).
- [44] D. Urzagasti, B.A. Vargas, L.A. Quispe-Flores, «Chaotic one-dimensional domains induced by periodic potentials in normal-dispersion fiber lasers», *Chaos* **27**, 103116 (2017).
- [45] T.P. Horikis, H.E. Nistazakis, «Dynamical oscillations in nonlinear optical media», *Optics Commun.* **283**, 1467 (2010).
- [46] H. Sakaguchi, B.A. Malomed, «Resonant nonlinearity management for nonlinear Schrödinger solitons», *Phys. Rev. E* **70**, 066613 (2004).
- [47] G.C. Katsimiga *et al.*, «Dark–bright soliton dynamics beyond the mean-field approximation», *New J. Phys.* **19**, 073004 (2017).
- [48] J. Belmonte-Beitia, V.M. Pérez-García, V. Vekslerchik, V.V. Konotop, «Localized Nonlinear Waves in Systems with Time- and Space-Modulated Nonlinearities», *Phys. Rev. Lett.* **100**, 164102 (2008).
- [49] F.K. Abdullaev, J. Garnier, «Propagation of matter-wave solitons in periodic and random nonlinear potentials», *Phys. Rev. A* **72**, 061605 (2005).
- [50] I.V. Barashenkov, M.M. Bogdan, V.I. Korobov, «Stability Diagram of the Phase-Locked Solitons in the Parametrically Driven, Damped Nonlinear Schrödinger Equation», *Europhys. Lett.* **15**, 113 (1991).
- [51] M.G. Clerc, S. Coulibaly, D. Laroze, «Interaction law of 2D localized precession states», *Europhys. Lett.* **90**, 38005 (2010).
- [52] D. Anderson, «Variational approach to nonlinear pulse propagation in optical fibers», *Phys. Rev. A* **27**, 3135 (1983).
- [53] F.G. Mertens, N.R. Quintero, A.R. Bishop, «Nonlinear Schrödinger equation with spatiotemporal perturbations», *Phys. Rev. E* **81**, 016608 (2010).
- [54] R. Scharf, A.R. Bishop, «Soliton chaos in the nonlinear Schrödinger equation with spatially periodic perturbations», *Phys. Rev. A* **46**, R2973 (1992).
- [55] V. Seghete, C.R. Menyuk, B.S. Marks, «Solitons in the midst of chaos», *Phys. Rev. A* **76**, 043803 (2007).
- [56] Z. Wang *et al.*, «Chaotic Spin-Wave Solitons in Magnetic Film Feedback Rings», *Phys. Rev. Lett.* **107**, 114102 (2011).
- [57] A.B. Ustinov *et al.*, «Observation of the Chaotic Spin-Wave Soliton Trains in Magnetic Films», *Phys. Rev. Lett.* **106**, 017201 (2011).
- [58] N. Akhmediev, J.M. Soto-Crespo, G. Town, «Pulsating solitons, chaotic solitons, period doubling, and pulse coexistence in mode-locked lasers: Complex Ginzburg–Landau equation approach», *Phys. Rev. E* **63**, 056602 (2001).
- [59] P. Müller, F.G. Mertens, A.R. Bishop, «Chaotic transport in deterministic sine-Gordon soliton ratchets», *Phys. Rev. E* **79**, 016207 (2009).
- [60] J.M. Soto-Crespo, N. Akhmediev, «Soliton as Strange Attractor: Nonlinear Synchronization and Chaos», *Phys. Rev. Lett.* **95**, 024101 (2005).

- [61] W.C.K. Mak, B.A. Malomed, P.L. Chu, «Interaction of a soliton with a localized gain in a fiber Bragg grating», *Phys. Rev. E* **67**, 026608 (2003).
- [62] J. Cuevas, B. Sánchez-Rey, M. Salerno, «Regular and chaotic transport of discrete solitons in asymmetric potentials», *Phys. Rev. E* **82**, 016604 (2010).
- [63] A.D. Martin, C.S. Adams, S.A. Gardiner, «Bright Matter-Wave Soliton Collisions in a Harmonic Trap: Regular and Chaotic Dynamics», *Phys. Rev. Lett.* **98**, 020402 (2007).
- [64] G.J. de Valcárcel, I. Pérez-Arjona, E. Roldán, «Domain Walls and Ising–Bloch Transitions in Parametrically Driven Systems», *Phys. Rev. Lett.* **89**, 164101 (2002).
- [65] D. Urzagasti *et al.*, «Two-soliton precession state in a parametrically driven magnetic wire», *J. Appl. Phys.* **111**, 07D111 (2012).
- [66] M.G. Clerc, S. Coulibaly, D. Laroze, «Nonvariational Ising–Bloch Transition in Parametrically Driven Systems», *Int. J. Bifur. Chaos* **19**, 2717 (2009).
- [67] A. Sánchez, R. Scharf, A.R. Bishop, L. Vázquez, «Sine-Gordon breathers on spatially periodic potentials», *Phys. Rev. A* **45**, 6031 (1992).
- [68] H. Goldstein, C.P. Poole, J.L. Safko, «Classical Mechanics. 3rd Ed.», *Addison-Wesley*, 2001.
- [69] I.V. Barashenkov, S.R. Woodford, E.V. Zemlyanaya, «Interactions of parametrically driven dark solitons. I. Néel–Néel and Bloch–Bloch interactions», *Phys. Rev. E* **75**, 026604 (2007).
- [70] E.N. Tsoy, A. Ankiewicz, N. Akhmediev, «Dynamical models for dissipative localized waves of the complex Ginzburg–Landau equation», *Phys. Rev. E* **73**, 036621 (2006).
- [71] R.J. Deissler, «External noise and the origin and dynamics of structure in convectively unstable systems», *J. Stat. Phys.* **54**, 1459 (1989).
- [72] W.L. Ditto *et al.*, «Experimental observation of a strange nonchaotic attractor», *Phys. Rev. Lett.* **65**, 533 (1990).
- [73] G.M. Zaslavskii, R.Z. Sagdeev, D.K. Chaikovskii, A.A. Chernikov, «Chaos and two-dimensional random walk in periodic and quasiperiodic fields», *Zh. Eksp. Teor. Fiz.* **95**, 1723 (1989).